

## C-D1. Simulation and design of collector array units within large systems

### IEA SHC FACT SHEET 55.C.D.1.4.

|                       |                                                                                           |
|-----------------------|-------------------------------------------------------------------------------------------|
| Subject:              | CFD models of different collector types                                                   |
| Description:          | CFD models of different collector types                                                   |
| Date:                 | 21.10.2019                                                                                |
| Authors:              | Jianhua Fan, Weiqiang Kong, Simon Furbo                                                   |
| Download possible at: | <a href="http://task55.iea-shc.org/fact-sheets">http://task55.iea-shc.org/fact-sheets</a> |

### Introduction

By the end of 2017, solar heating plants with a total surface of more than 1.3 million m<sup>2</sup> were in operation in Denmark. Most solar collectors in the existing solar heating plants are typically flat plate collectors (FPC).

Fan and Furbo and Furbo et al. [1], [2] investigated heat transfer and fluid flow in a large flat plate solar collector designed for solar heating plants. The FPC is especially designed for district heating applications with operation temperatures in the range 40-95°C. The collector is characterized by a maximum collector efficiency up to 83-85% and a heat loss coefficient as low as 3 W/m<sup>2</sup>/K. CFD calculations were carried out to investigate the influence of uneven flow distribution on collector efficiency and temperature distribution. Risk of local overheating was identified.

The efficiency of flat plate collectors decreases significantly in the range of 70°C-95°C, while parabolic-trough collectors (PTC) and compound parabolic collector (CPC) keep relatively high efficiency in the range of 70°C - 95°C. It is therefore advantageous to use CPC and/or PTC in a solar district heating plant for the temperature range between 70°C-95°C.

Craig et al. [3] evaluated the use of CFD to investigate solar irradiation of a concentrated solar collector without using the traditional ray-tracing methods. For all the test cases, good agreement was found when suitable modelling settings were used to limit both ray-effect and false scattering errors. Antonelli et al. [4] analyzed heat losses from compound parabolic collectors by CFD simulation. Antonin et al. [5] described CPC designs as primary concentrators for CPV. Both 2D and 3D CPC structures were evaluated and some particular solutions were selected for possible photovoltaic applications.

A new type of CPC collector has been developed by PolyCSP ApS for solar heating plants. The design of the CPC collector is especially optimized for the temperature range of 90-160 °C. The main components of the CPC collector are the new "POLYCSP" absorber tubes in combination with multi-parabolic receivers, all

## C-D1. Simulation and design of collector array units within large systems

integrated in a robust flat panel design (Sallaberry et al. 2017). Inside the metal absorber tube there is a metal tube of a smaller diameter. Collector fluid is circulated through the annulus in between the two co-axial tubes. The aim of the design is to increase the convective heat transfer between the absorber and the collector fluid by creating turbulence in the tube. The unique design of the hybrid collectors enables significantly higher efficiencies than conventional flat plate collectors (FPC) and evacuated tubular collectors (ETC) at similar cost levels. At the same time the CPC collector enables higher operating temperatures and higher total energy output similar to the more costly PTC and Linear Fresnel Reflector (LFR) systems, however with the robustness and simplicity similar to the conventional flat plate panels.

The newly developed CPC collector was tested in an outdoor test facility in the campus of the Technical University of Denmark. Detailed measurements were carried out to document the temperature increases of the collector under operation conditions. Collector efficiency was determined for different operation temperatures. The measured collector efficiencies and the measured temperatures were compared to the calculated ones by a simplified CFD model of the CPC collector. Validity of the CFD model is elucidated. The validated CFD model is then used to predict collector efficiency at higher temperatures above the limit of the test facility. An expression of efficiency for the CPC collector is then determined based on the CFD calculated efficiency points. The CFD model indicates a risk of local overheating due to uneven temperature distribution along the receiver tubes.

### CFD investigations on flat plate solar collectors

#### Flow distribution

Computational fluid dynamic investigations were carried out to study the uneven flow distribution in a large flat plate solar collector designed for solar heating plant (Fan and Furbo, 2007, 2008). Figure 1 shows the design of the 12.53 m<sup>2</sup> HTU flat-plate solar collector from Arcon-Sunmark A/S, Denmark. The collector panel is a high temperature solar collector designed for medium and large sized solar heating systems. The collector panel consists of two manifolds (one dividing and one combining flow manifold) and 16 parallel connected horizontal fins in a “U” type configuration, see Fig. 2. The length of the absorber strips is 5.79 m. The solar collector fluid divides from the dividing manifold into 16 strips.

## C-D1. Simulation and design of collector array units within large systems

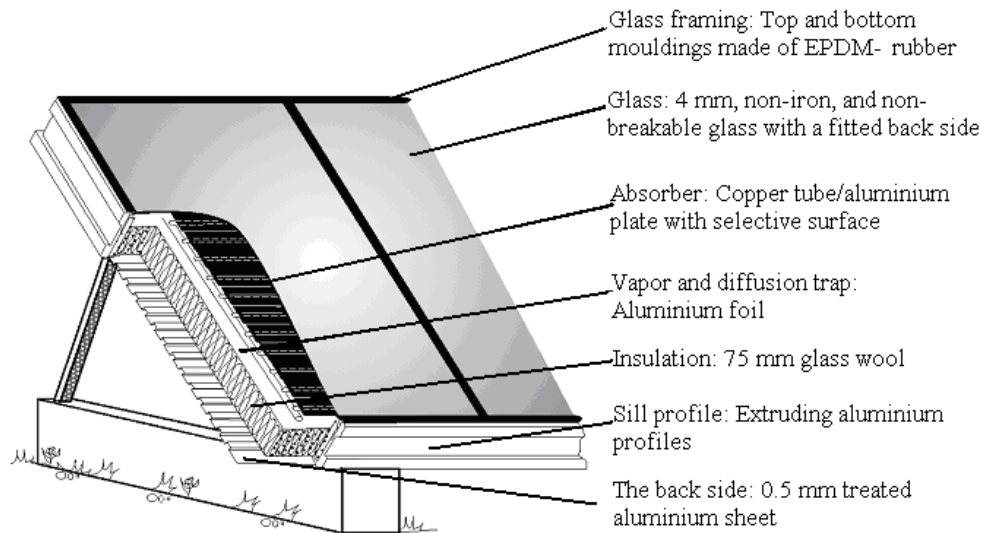


Fig. 1. Design of the investigated HTU solar collector.

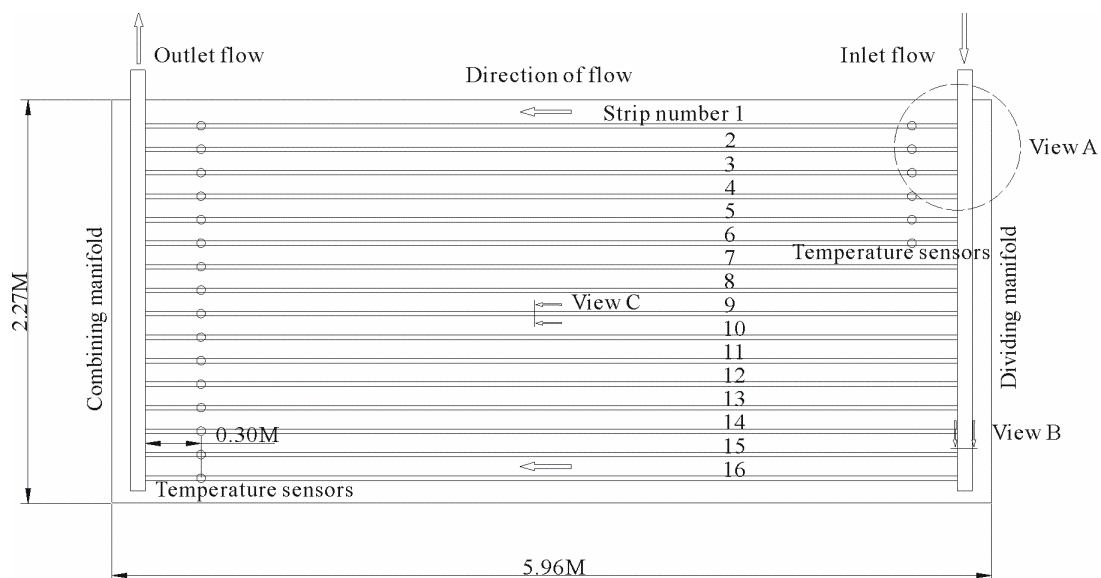


Fig. 2. A schematic illustration of the HTU solar collector configuration.

Fig. 3 shows a simplified CFD model of the flat plate solar collector. The absorbed solar energy is transferred from the fin to the tube walls and from the tube walls to the solar collector fluid. The temperature of the solar collector fluid will increase as it flows along the tube. The amount of energy transferred to the solar collector fluid and the fluid temperature will be influenced by the temperature of the absorber fin and the duration of the period the fluid stays in the tube. Consequently, the fluid flow rate

## C-D1. Simulation and design of collector array units within large systems

and the flow rate distribution will influence the collector fluid temperature distribution. If the collector fluid flow rate through the absorber tube is small, the fluid temperature will be relatively high just before the fluid enters the combining manifold, and vice versa.

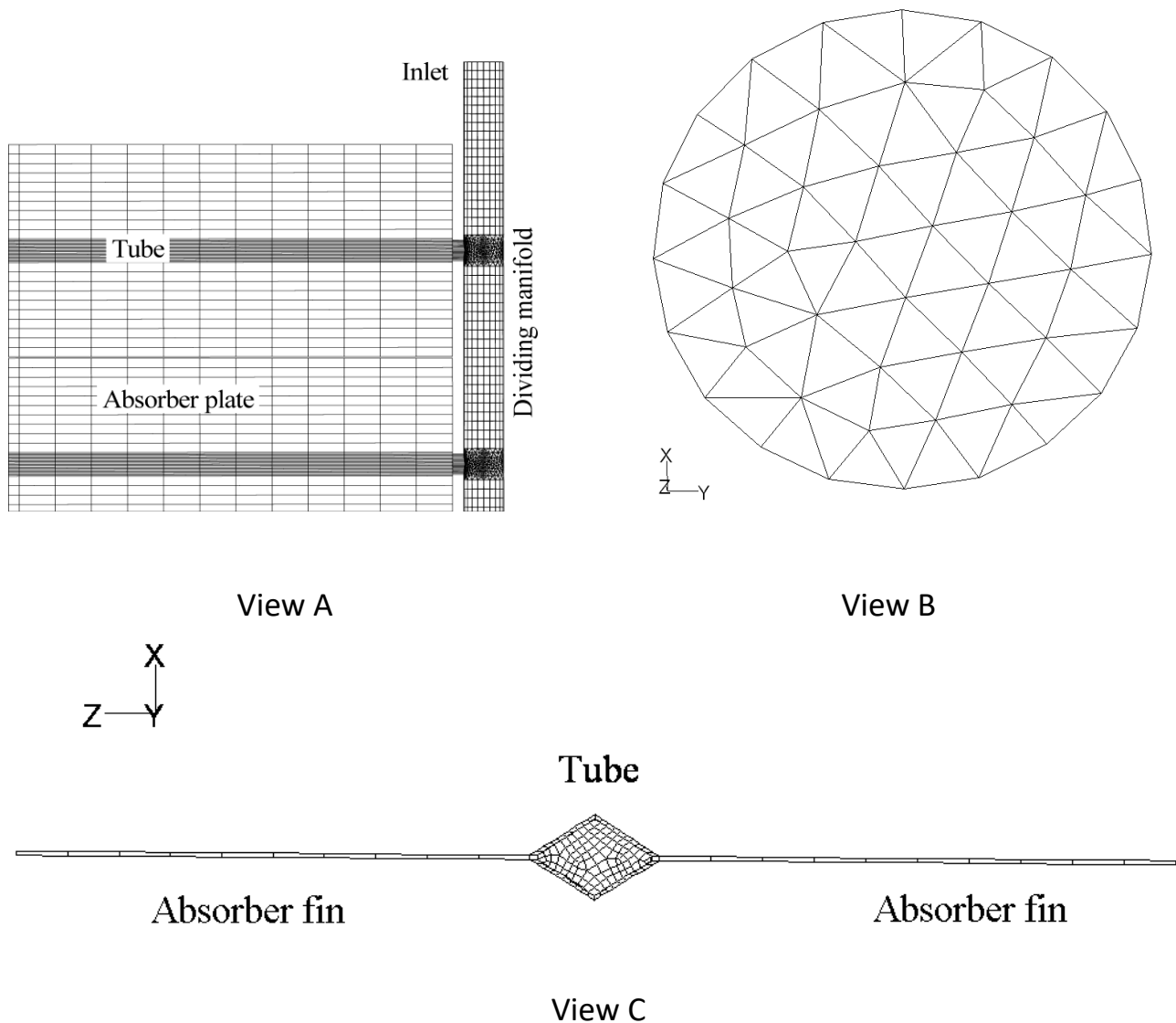


Fig. 3. A CFD model of the flat plate solar collector.

CFD-calculated flow and temperature distribution in the strips just before the fluid enters the combining manifold are shown in Fig. 4. The solar collector in question has an inlet flow rate of 2.7 l/min and an inlet fluid temperature of 19.4°C, and the collector is heated by a solar irradiance of 883 W/m<sup>2</sup>. An ambient air temperature of 21.7°C and a solar collector tilt of 40° are assumed. It can be seen that the flow distribution through the tubes is not uniform. The fluid flow rate in the strips increases from the top to the bottom. In

## C-D1. Simulation and design of collector array units within large systems

the top strip 1, the flow rate is 0.11 l/min, while in the bottom strip 16 the flow rate is 0.23 l/min, approx. twice of that in the top strip. This is due to the influence of buoyancy forces on the fluid flow distribution in the absorber strips. The buoyancy forces, caused by the cold dividing manifold on the right hand side and the warm combining manifold on the left hand side of the collector, tend to circulate clockwise in the collector panel thus decreasing flow rate in the upper absorber strips and increasing flow rate in the bottom absorber strips. With increase of the flow rate in the strip, the fluid temperature decreases from the top to the bottom. The fluid temperature just before the fluid enters the combining manifold can be as high as 86.6°C in the top strip 1 compared with a maximum temperature of 54.6°C in the bottom strip. The temperatures of the tube walls are approx. 5K higher than the collector fluid temperatures. It should be noted that all the temperatures are calculated by an average of all the computational cells at the cross section with cell masses weighted.

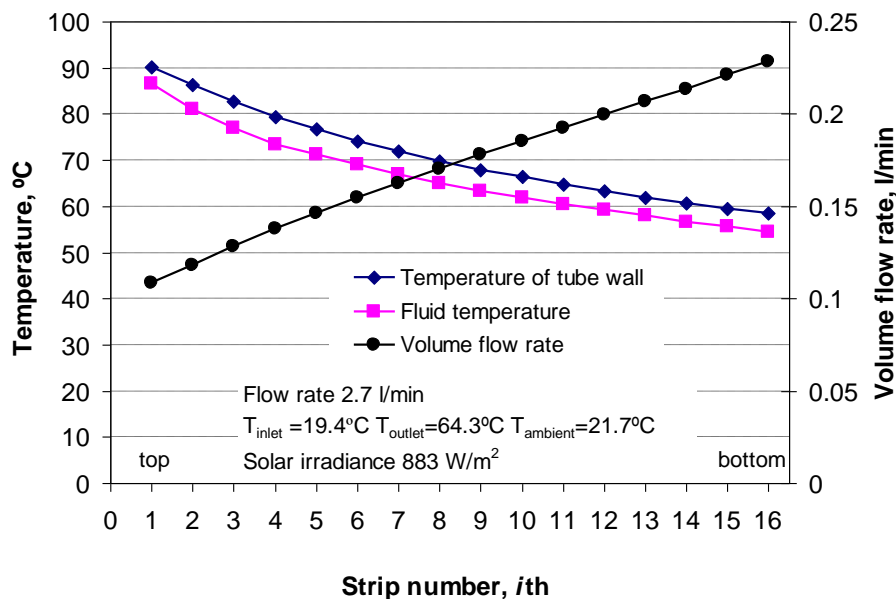


Fig. 4. Calculated temperature and volume flow rate distribution in the strips just before the fluid enters the combining manifold.

The temperature distribution at the middle plane of the absorber is presented in Fig. 5. For a solar collector with an inlet fluid temperature of 19.4°C and a collector fluid volume flow rate of 2.7 l/min, the flow distribution through the tubes is not uniform, which results in an uneven temperature distribution. Horizontally the temperature of the solar collector fluid in the tubes and the absorber fin temperature increase from the inlet side to the outlet side of the collector panel. Vertically the fluid and the absorber fin

## C-D1. Simulation and design of collector array units within large systems

temperatures in the upper part of the collector are relatively higher than those in the lower part, mainly due to the difference of the fluid flow rates in the strips. The outlet fluid temperature from the solar collector is approx. 64.5°C, while the minimum and the maximum temperature of the fluid just before it enters the combining manifold are 54.6°C and 86.6°C respectively, which are 9.9 K lower and 22.1 K higher than the outlet fluid temperature. An increase of the temperature from the collector fluid in the strips to the absorber fin can be seen as well in the temperature profile.

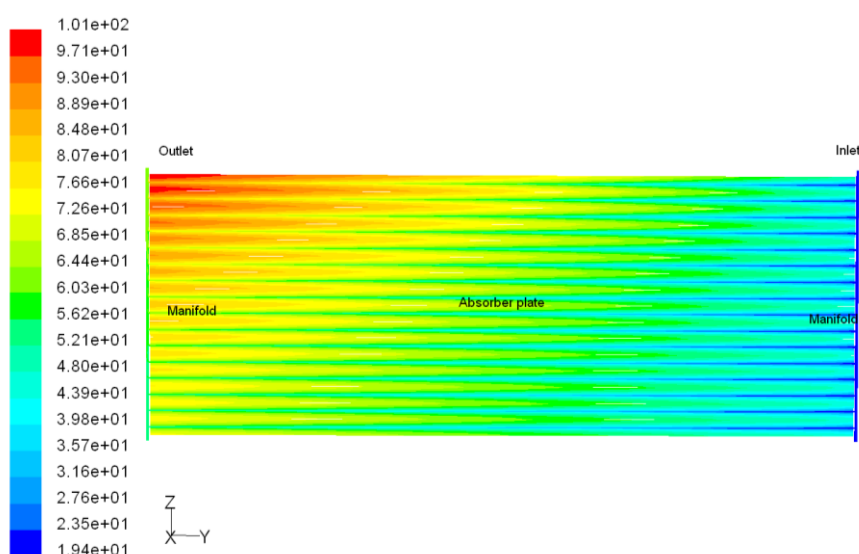


Fig. 5. CFD calculated temperature distribution (°C) at the middle plane of the absorber.

The flow distribution through the absorber tubes is examined experimentally by means of temperature measurements at the back of the absorber tubes. Measurements are carried out with different collector fluid volume flow rates, fluid inlet temperatures and under different weather conditions. Six cases are investigated, see table 1.

Table 1. Test conditions investigated.

| Case number | Collector fluid flow rate | Inlet fluid temperature | Outlet fluid temperature | Ambient air temperature | Solar irradiance |
|-------------|---------------------------|-------------------------|--------------------------|-------------------------|------------------|
| -           | l/min                     | °C                      | °C                       | °C                      | W/m <sup>2</sup> |
| 1           | 2.7                       | 19.4                    | 64.3                     | 21.7                    | 883              |
| 2           | 3.4                       | 20.0                    | 57.6                     | 24.5                    | 866              |
| 3           | 5.0                       | 41.2                    | 69.1                     | 27.8                    | 1000             |

## C-D1. Simulation and design of collector array units within large systems

|   |      |      |      |      |      |
|---|------|------|------|------|------|
| 4 | 4.9  | 68.7 | 89.9 | 27.8 | 919  |
| 5 | 10.2 | 85.9 | 93.4 | 25.3 | 822  |
| 6 | 24.3 | 86.7 | 91.3 | 22.7 | 1018 |

The measured tube wall temperatures are compared to the calculated tube wall temperatures by the CFD model. Figure 6. shows the comparison between the measured and the calculated tube wall temperatures at the joints where the strips meet the combining manifold. There is a good agreement between the measured and calculated temperatures except minor differences at the top one or two strips and the bottom two strips. One reason for the disagreement could be the effect of boundary conditions of these strips close to the top and bottom of the collector panel. Another reason could be the air flow circulation in the space between the cover and the absorber plate driven by the buoyancy effects due to the temperature difference between the warm air at the outlet side of the collector and the colder air at the inlet side of the collector. The air circulating clockwise in the collector panel will bring warm air to the top of the collector panel and cold air to the bottom of the collector panel.

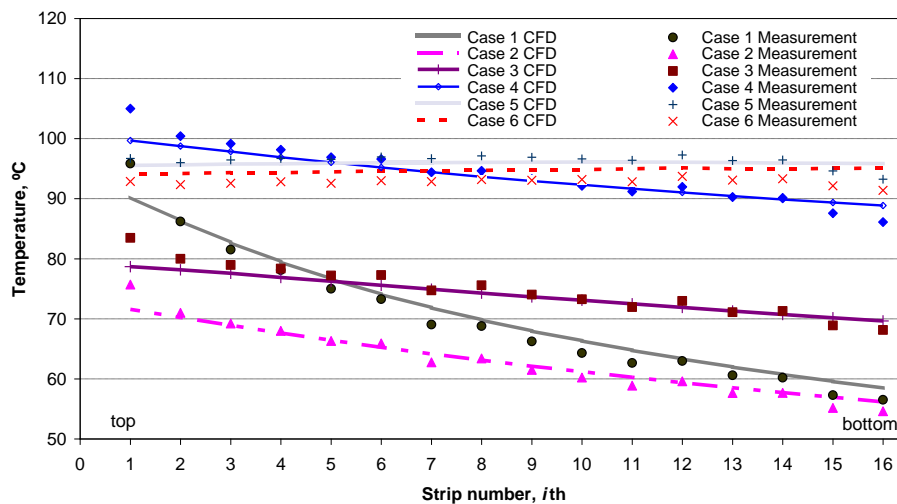


Fig. 6. Measured and calculated tube wall temperatures at the joints where the strips meet the combining manifold.

### Influence on efficiencies

The uneven flow and temperature distribution in the collector panel will decrease the collector efficiency. Fig. 7 shows the CFD calculated collector efficiency at different collector volume flow rates, Fan et al. [6]. Boiling is not considered in the CFD calculations. The Reynolds number of the fluid flow in the tube will be in the range of 265 – 2000 for a volume flow rate between 3.3 l/min and 25.0 l/min if a solar collector fluid

## C-D1. Simulation and design of collector array units within large systems

of 40% glycol water mixture and a mean collector fluid temperature of 60°C are used. Therefore, a laminar flow model is used in the CFD calculations. Based on the CFD calculated efficiencies, a regression analysis is carried out to find the efficiency expressions of the collector at an incidence angle of 0° operating at different fluid flow rates (see the following table):

$$\eta = \eta_0 - a_1 \frac{T_m - T_a}{G} - a_2 \frac{(T_m - T_a)^2}{G} \quad (1)$$

Table 2. Collector efficiencies at different flow rates.

| Flow rate | 3.3 l/min                       | 4.0 l/min | 6.0 l/min | 10.0 l/min | 25.0 l/min |      |
|-----------|---------------------------------|-----------|-----------|------------|------------|------|
| $\eta_0$  | -                               | 0.82      | 0.82      | 0.82       | 0.81       |      |
| $a_1$     | W/m <sup>2</sup> K              | 4.63      | 4.55      | 4.32       | 4.34       | 4.64 |
| $a_2$     | W/m <sup>2</sup> K <sup>2</sup> | 0.009     | 0         | 0          | 0          | 0    |

It can be seen that collectors at flow rates of 6.0 l/min and 10.0 l/min give the highest performance, while collectors at flow rates of 3.3 l/min and 25.0 l/min give lower efficiency. This is due to the uneven flow distribution when the flow rate is too high or too low. The relative flow nonuniformity for flow rates of 3.3 l/min and 25.0 l/min are 40.2% and 7.8% respectively. If the flow rate is low enough, the flow nonuniformity will dramatically increase resulting in an increased collector mean temperature and a decreased collector efficiency. For high flow rates (>10.0 l/min), the flow nonuniformity will also increase resulting in a decreased collector efficiency. Besides the flow distribution problems, the air temperature distribution inside the collector panel, which varies for different collector volume flow rates, will also influence collector efficiency. That is the reason why the collector efficiency is relatively low at the flow rate of 25.0 l/min. However, if the flow rate is higher than 25.0 l/min, the fluid flow in the tubes will normally be turbulent. For such high flow rates, the collector efficiency will have a sharp increase because the heat transfer coefficient from the tube wall to the fluid will increase dramatically as the fluid flow transits from the laminar to the turbulent region.

## C-D1. Simulation and design of collector array units within large systems

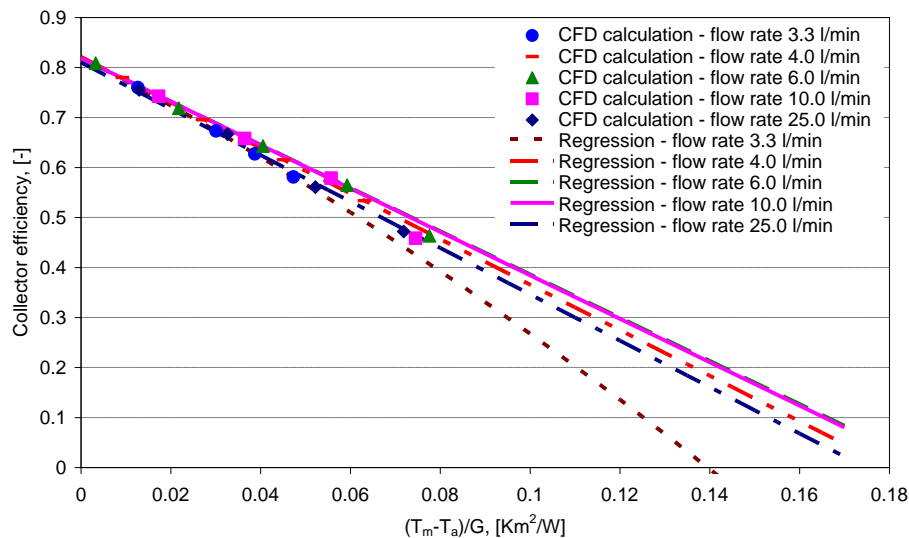


Fig. 7. the CFD calculated collector efficiency and the efficiency expression at different collector fluid flow rates.

### CFD investigations on CPC solar collectors

A 15.4 m<sup>2</sup> PolyCSP CPC solar collector was tested at the campus of the Technical University of Denmark in September 2016, see Fig. 8 (Yuan et al, manuscript submitted). In the test platform two collectors were tested side by side. The two collectors are identical except that one of the collectors is equipped with a transparent ETFE (Ethylene tetrafluoroethylene) foil and the other collector is not. The focus of the paper is the collector without ETFE foil, shown as the left collector in Fig. 8. The solar collector is designed and manufactured by the Danish company PolyCSP ApS for medium and large solar heating systems. The collector consists of four identical parabolic-troughs with a width of 0.616 m and a length of 5.9 m. Fig. 9 shows a view of the collector panel from the side. The gross area and the aperture area of the collector are 15.4 m<sup>2</sup> and 13.9 m<sup>2</sup> respectively. The parabolic troughs are covered by a glass cover at the front and insulated by mineral wool at the back. The parabolic shaped reflector concentrates solar rays passing the glass cover on a metal tube with selective coating on the outer surface of the tube. The outer diameter and wall thickness of the tube are 48 mm and 2 mm respectively. Inside the outer tube there is another metal tube with an outer diameter of 40 mm. In the annulus between the two metal tubes a propylene glycol water mixture is circulated to remove heat from the tube wall. The collector is oriented in the East-West direction. The whole collector panel is placed on a one-axis tracker that automatically adjusts the tilt of the collector panel to track the sun.

## C-D1. Simulation and design of collector array units within large systems



Fig. 8 Photo of the new CPC solar collectors and the test rig.

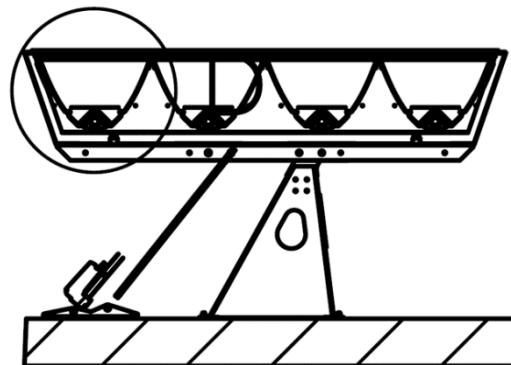


Fig. 9 schematic illustration of the collector panel design.

The thermal performance of the CPC solar collector panel was investigated numerically by CFD simulations Yuan et al. [7] (manuscript submitted). A simplified CFD model of the collector is built using Ansys Fluent 17.0 Ansys Fluent [8]. Preliminary investigations indicate that there are even flow distributions among the four identical parabolic-troughs, therefore periodic thermal conditions for the trough are assumed. The collector panel could be simplified to one parabolic trough with a periodic boundary condition on both sides of the trough, see Fig. 10. The dimension of the trough is 5900 mm long, 616 mm wide and 458 mm tall, which is the same as for the tested collector. In this way computing time consumption is significantly reduced without sacrificing validity of the model. The CFD model includes the parabolic reflector, the metal tube with a wall thickness, the glass cover at the front and insulation material at the back, therefore the CFD model is able to calculate not only air movement in the solar collector panel but also the turbulent water flow in the absorber

## C-D1. Simulation and design of collector array units within large systems

tubes. In term of heat transfer, the conjugate heat transport between fluid and solid material, the convective heat transport in fluid regions and thermal radiation are calculated in the CFD model.

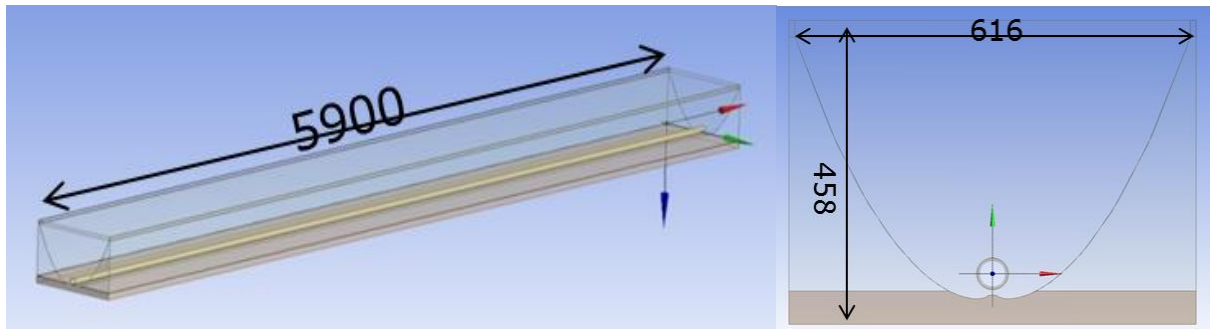


Fig. 10 The simplified CFD model of the CPC solar collector (figure to the right, cross section view of the trough).

With the beam solar radiation on the receiver surface, the inlet temperature of the collector and the ambient air temperature as inputs, the CFD model calculates the convective heat transfer between the receiver and the solar collector fluid, the conductive heat transfer along the receiver tube and the radiation and convective heat transfer between the receiver surface and the rest of the collector. Fluid dynamics of both the solar collector fluid in the tube and the air inside the collector panel are calculated.

Fig. 11 shows the temperature distribution on the tube receiver surface for a beam irradiance of  $895 \text{ W/m}^2$ , a diffuse radiation of  $95 \text{ W/m}^2$  and a mean solar collector temperature of  $80.7^\circ\text{C}$ . Temperatures of the tube receiver surface are shown versus the angle at different distances from the inlet. The angle is determined by moving along the receiver surface in the clockwise direction from the furthest point to the left. The plot at  $0.1 \text{ m}$  from the inlet shows a lower temperature of around  $76.5\text{--}77.5^\circ\text{C}$  in the angles between  $50\text{--}120^\circ$  and  $180\text{--}360^\circ$ , which corresponds well to the distribution pattern of the beam solar radiation on the receiver surface. The surface temperature could be lower than the inlet temperature of the collector  $76.8^\circ\text{C}$ , due to cooling of the surface by convection and thermal radiation. There are two peaks of surface temperatures: one at an angle of  $32\text{--}39^\circ$  and the other one at an angle of  $140^\circ$ .

With an increase of distance from the inlet, the peak temperatures of the receiver surface increase due to heating by concentrated solar radiation except in the area with an angle in between  $220\text{--}336^\circ$ . Since the beam solar radiation is very low in that part of the receiver surface, the surface temperature can be lower than the inlet temperature due to heat loss from the surface. At a distance of  $1.5 \text{ m}$  from the inlet, the lowest temperature of the receiver surface reaches  $75^\circ\text{C}$ , which is  $1.8 \text{ K}$  lower than the inlet temperature.

## C-D1. Simulation and design of collector array units within large systems

At the point 5.8 m from the inlet (0.1 m to the outlet), two peak temperatures can be seen around the receiver surface, 90.6°C at an angle of 32-39° and 93.8°C at an angle of 140°. Although the peak of beam solar radiation at 36° (37734 W/m<sup>2</sup>) is slightly higher than the peak at 140° (37010 W/m<sup>2</sup>), the peak surface temperature at 32-39° is 3.2 K lower than the peak surface temperature at 140°. It can be explained by the tilt of the collector, which is 51.3° in the calculation. The gravity direction corresponds to the outgoing direction at an angle of 321.3° (indicated as G in Fig. 11). Due to buoyancy driven flow, warm fluid tends to rise up to the upper part of the tube. The conjugate effect of the buoyancy driven force and the beam solar irradiance results in a higher surface temperature around an angle of 140°.

The results show that there is a significant temperature difference along the tube both in the axial and in the tangential directions of the tube, which could cause the risk of local boiling at the upper part of the tube close to the outlet of the collector. Another reason of the large temperature difference is the material property of the receiver tube. The receiver tube is made of stainless steel which has a lower thermal conductivity. If material with a higher thermal conductivity for example copper is used as material of the tube, the temperature difference along the tube will be smaller.

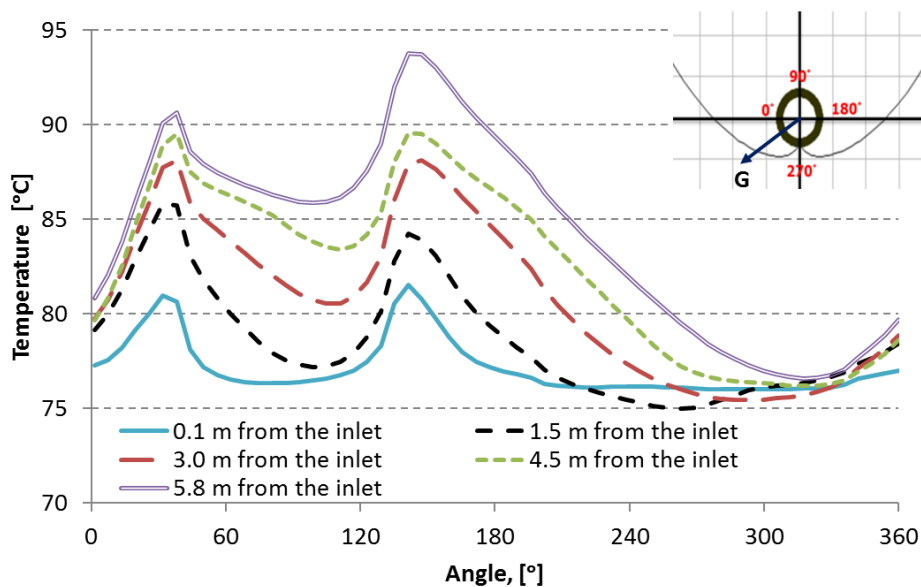


Fig. 11 Calculated temperature distribution on the tube receiver surface for an irradiance of 895 W/m<sup>2</sup> and a mean solar collector temperature of 80.7°C.

## C-D1. Simulation and design of collector array units within large systems

The CFD calculated collector efficiencies were plotted versus the temperature difference of the collector  $(T_m - T_a)/G_t$ , as shown in red squares in Fig. 12 (Yuan et al, manuscript submitted). The collector efficiency expression was determined using a regression based on the CFD predicted efficiency points.

The peak collector efficiency of the CPC solar collector is 57%, which is lower than a typical flat plate solar collector but the heat loss coefficients of the collector are much lower than for a typical flat plate solar collector. The lower peak collector efficiency could be explained by tracking error, surface accuracy of the reflectors and the incapability to utilize diffuse solar radiation. The lower heat loss coefficients of the CPC collector are due to the much smaller area of the absorber surface where heat is lost to the ambient, better insulation at the back of the panel and glass cover in the front of the panel.

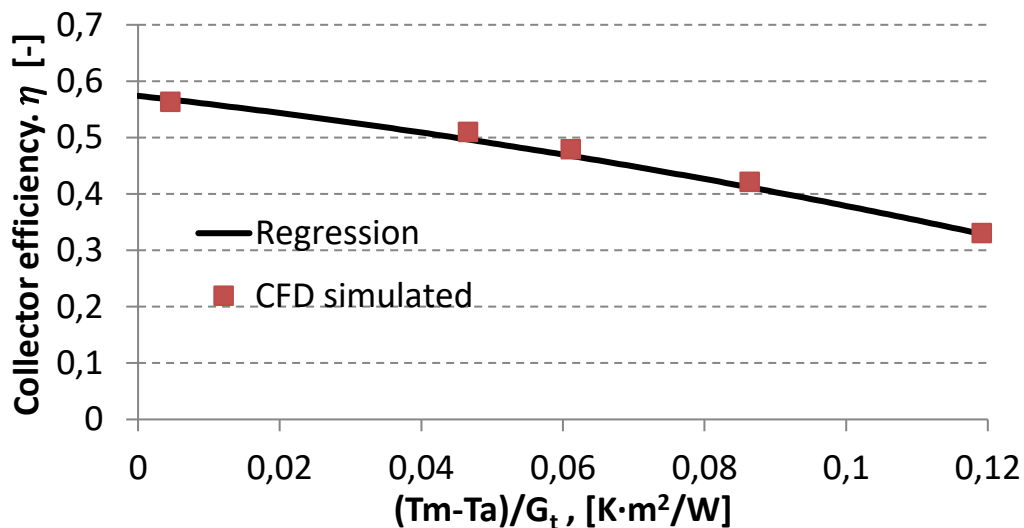


Fig. 12 CFD predicted collector efficiency expression.

Fig. 13 shows the CFD calculated temperatures in °C on a plane perpendicular to the tube. The section plane is located in the middle of the tube. Temperature plots on two interior CPC rows are obtained based on the calculation on one CPC row due to the periodic condition of the interior CPC collector row. In the calculation the beam solar irradiance was 895 W/m<sup>2</sup>. The inlet temperature of the collector and the ambient temperature were 77 °C and 26 °C respectively. The calculation shows that in the annulus between the tubes the fluid is heated by the absorbed solar energy to a temperature of around 80 °C. Air around the tube is heated by the receiver surface, creating a rising air flow with a relatively higher temperature than the average air temperature in the collector panel. The uprising warm air reaches the CPC mirror surface and flows along the mirror surface up to the glass cover. There is a gap of 25 mm between the glass cover and the mirror. The uprising warm air flows along the glass cover upwards. Due to the periodic boundary conditions, there is also an uprising air flow at the lower gap between the glass cover and the mirror. An uprising flow along

## C-D1. Simulation and design of collector array units within large systems

the glass cover can be seen in the area close to the glass cover, see Fig. 14. The uprising flow along the mirror collides with the uprising flow along the glass cover, creating two circulations in the middle of the collector.

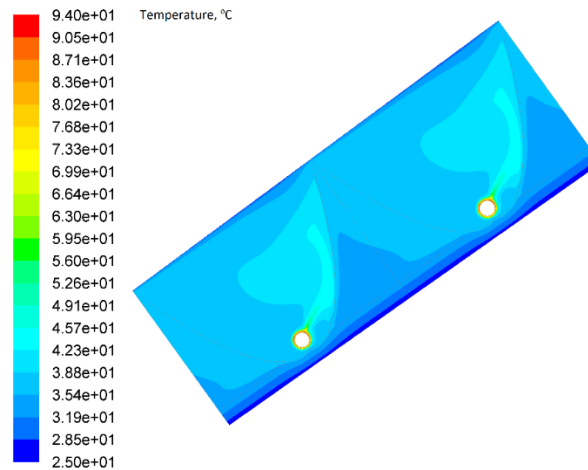


Fig. 13 CFD calculated temperatures in °C on the middle plane perpendicular to the tube showing two interior CPC rows.

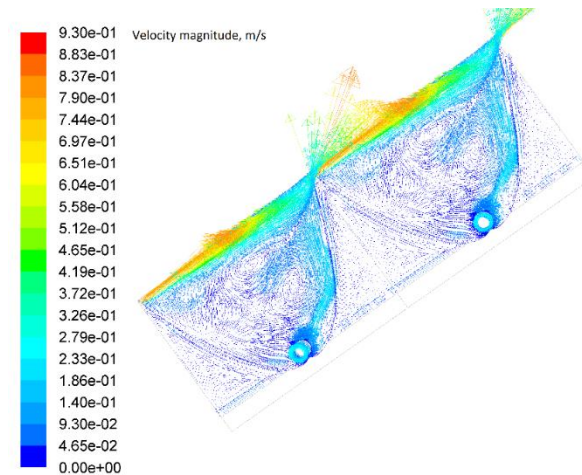


Fig. 14 CFD calculated velocity vectors in m/s on the middle plane perpendicular to the tube showing two interior CPC rows.

### Conclusions

Theoretical and experimental investigations were carried out to determine the thermal performance of a new 15.4 m<sup>2</sup> compound parabolic concentrator (CPC) solar collector and a 12.5 m<sup>2</sup> flat plate solar collector. Simplified CFD models of the CPC collector and of the flat plate solar collector were developed and

## C-D1. Simulation and design of collector array units within large systems

validated by the measurements. The validated CFD models will be used in future investigations with an aim to optimize the design of the collectors.

### References

- [1] Fan J., Shah L.J., Furbo S. Flow distribution in a solar collector panel with horizontally inclined absorber strips. *Solar Energy*, 81(2007), 1501-1511.
- [2] Fan J., Furbo S. Buoyancy effects on thermal behavior of a flat-plate solar collector. *Journal of Solar Energy Engineering*, 130(2008), 021010.
- [3] Craig K.J., Moghimi M.A., Rungasamy A.E., Marsberg J., Meye J.P. Finite-volume ray tracing using Computational Fluid Dynamics in linear focus CSP applications. *Applied Energy* 183 (2016) 241–256.
- [4] Antonelli M., Francesconi M., Marco P.D., Desideri U. Analysis of heat transfer in different CPC solar collectors: A CFD approach. *Applied Thermal Engineering* 101 (2016) 479–489
- [5] Antonin A., Stefancich M., Coventry J., Parretta A. Modelling of Compound Parabolic Concentrators for Photovoltaic Applications. *International Journal of Optics and Applications* 3(4) (2013): 40-52
- [6] Fan J., Shah L.J., Furbo S. The Effect of the Volume Flow rate on the Efficiency of a Solar Collector. EuroSun (2006), Glasgow, United Kingdom.
- [7] Yuan Guofeng, Fan J., Kong W., Furbo S., Perers B., Sallaberry F., Experimental and Computational Fluid Dynamics Investigations of a CPC Solar Collector for District Heating, *Applied Thermal Engineering*, Submitted
- [8] Ansys Inc., 2016. Ansys Fluent release 17.0, Southpointe, 2600, Ansys Drive, Canonsburg, PA 15317, USA.